Final Technical Report

Identification #- DE-FC26-04NT42324

Program: "Thermotunneling Based Cooling Systems for High Efficiency Buildings"

NETL Project Manager: Ryan Egidi

Recipient: GE Global Research

Contract Contact: Jeff Popielarczyk

Principal Investigator: Stan Weaver

Contributing Authors: Marco Aimi, Mehmet Arik, James Bray, Thomas Gorczyca, Darryl Michael, and Stan Weaver

Objective:

GE Global Research's overall objective was to develop a novel thermotunneling-cooling device. The end use for these devices is the replacement of vapor cycle compression (VCC) units in residential and commercial cooling and refrigeration systems.

Thermotunneling devices offer many advantages over vapor cycle compression cooling units. These include quiet, reliable, non-moving parts operation without refrigerant gasses. Additionally theoretical calculations suggest that the efficiency of thermotunneling devices can be 1.5-2x that of VCC units. Given these attributes it can be seen that thermotunneling devices have the potential for dramatic energy savings and are environmentally friendly.

A thermotunneling device consists of two low work function electrodes separated by a sub 10 nanometer-sized gap. Cooling by thermotunneling refers to the transport of hot electrons across the gap, from the object to be cooled (cathode) to the heat rejection electrode (anode), by an applied potential. GE Global Research's goal was to model, design, fabricate devices and demonstrate cooling base on the thermotunneling technology.

Rationale and Anticipated Program Benefits:

DISCLAIMER

This report was prepared as an account of work sponsored by an agency of the United States Government. Neither the United States Government nor any agency thereof, nor any of their employees, makes any warranty, express or implied, or assumes any legal liability or responsibility for the accuracy, completeness, or usefulness of any information, apparatus, product, or process disclosed, or represents that its use would not infringe privately owned rights. Reference herein to any specific commercial product, process, or service by trade name, trademark, manufacturer, or otherwise does not necessarily constitute or imply its endorsement, recommendation, or favoring by the United States Government or any agency thereof. The views and opinions of authors expressed herein do not necessarily state or reflect those of the United States Government or any agency thereof.

At the initiation of this program residential energy usage associated with cooling equipment and refrigeration accounted for 3.36 quads, at a cost of more than $8.23 billion annually. Commercial cooling equipment and refrigeration totals 1.94 quads, at a cost of more than $4.75 billion annually.[11] VCC technology with a Carnot efficiency of 40–45% is used in nearly all existing cooling and refrigeration applications. The efficiency of this technology has seen only incremental improvements in the past 20 years. Breakthrough technologies in this area will have a major impact on energy savings and economic gains.

Thermotunneling cooling devices have the potential to offer a 1.5–2x increase in energy efficiency. Furthermore, the solid-state approach offers extreme reliability due to its operation without moving parts or compressed refrigerant. Without a need for refrigerant, thermotunneling devices are environmentally friendly and unaffected by low refrigerant levels that can degrade compressor efficiency and add to maintenance costs. Unlike VCC-based systems, thermotunneling devices are orientation insensitive, allowing totally new design concepts.

Theoretical modeling has shown that solid-state cooling based on thermotunneling devices has the potential to achieve Carnot efficiencies as high as 80% at cooling densities greater than 100 W/cm^2.[2,3] Attaining an estimated Carnot efficiency of 65% will result in a 44% improvement over VCCs. However, at the system level, the compression cycle accounts for 80% of the total energy usage in current cooling or refrigeration applications. The remaining 20% is consumed in ancillaries such as heat exchangers, circulating fans, controls, and internal cabinet lighting. It is anticipated that these ancillary losses will still exist in a thermotunneling-based refrigeration system. Therefore, the total realized efficiency gain in a cooling or refrigeration system is on the order of 35%.

Thermotunneling cooling devices are expected to be lower in cost than comparable VCC units. The initial cost of a VCC unit for refrigeration is approximately $2/W of cooling power. Based on the current passive thermotunneling concepts that utilize standard semiconductor batch fabrication,

the estimated cost is $0.10/W of cooling power. This estimate assumes a semiconductor build cost of $9/cm^2 [12] and a maximum attainable cooling power of 100 W/cm^2. System integration of thermotunneling devices will use current commercially available heat exchanger technologies. A fan blown heat sink assembly costs $0.15–0.20/W in bulk quantities.[13] Since the thermal interfaces are vital in the assembly, thermal interface materials will be utilized between the heat sink and thermal tunneling devices. The average cost of an interface material is $2/cm^2. Approximately 2 cm^2 of interface material is needed for a 200 W module. Since, the system will require two-sided thermal management (i.e., for both refrigerated surface and heat removal surface), total cost of heat sink and thermal interface materials is expected to be $0.308–0.408/W. The total cost of a thermal tunneling subsystem will be approximately $0.408–0.508/W. Therefore the solid-state refrigeration will be available at 20–25% of the current VCC refrigeration system cost. A low cost solid-state refrigeration system is critical to market acceptance, as consumers are less likely to pay a premium for energy savings.

Historical trends show that market penetration in commercial applications will lead to residential applications, where the payback period is a predominant factor. Thermotunneling-based refrigeration and cooling devices are expected to command a sizeable commercial market penetration due to their low cost of operation. Quad saving estimates for commercial and residential installations were calculated by: *system-level energy savings* x *national energy consumption* x *max. potential market penetration.* The maximum potential market penetration for commercial installations was calculated by: *1/average equipment lifetime* x *national energy consumption* x *percentage of units replaced with thermotunneling units.* The thermotunneling replacement percentage was arrived at using a judgmental method and was set to 70% for commercial cooling equipment. Residential quad saving estimates were made based on readily available data that is based on appliance lifetimes, total number of households, and appliance saturation levels. The maximum potential market penetration for residential

installations is calculated by: *total number of households* x *appliance saturation level* x *1/average equipment lifetime* x *percentage of units replaced with thermotunneling units.*

The thermotunneling replacement percentage was arrived at using a judgmental method and varied from 45–75% based on the particular appliance. Remodeling purchases have not been taken into account. By using these factors, the estimated first year savings for commercial cooling and refrigeration is 0.119 quads and the residential savings would be 0.0538 quads, for a total of 0.1728 quads or $0.42 billion. Estimated savings over the next ten years, assuming zero growth, would be 5.36 quads or $13.13 billion. The applications and potential for energy savings from thermotunneling-based cooling systems is dramatic.

The primary environmental benefit from the proposed thermotunneling devices will be a reduction in power plant generation commensurate with a reduction in power plant emissions. Total energy savings are estimated at 0.119 quads, giving a corresponding annual reduction in carbon emission of 2.71 billion kg. The impact of refrigeration and cooling systems on the stratospheric ozone layer is related to the release of ozone depleting refrigerants. Initial leakages occur during charging, normal operation, maintenance, and at disposal.[14] These refrigerants, combined with the emission of greenhouse gases, contribute to global warming. Thermotunneling devices utilize a vacuum or inert gas, thus totally eliminating the need for refrigerants. Additionally, the reduced volume and increased reliability of a thermotunneling device, while providing the same cooling power as a VCC system, will ultimately reduce landfill contributions. Another benefit is the reduction in external and internal building noise due to the thermotunneling devices silent operation resulting from nonmoving parts.

The market potential for thermotunneling-based solid-state systems covers a broad range of cooling and power generation applications. The previous discussions have been limited to cooling applications, however thermotunneling modules can be utilized as efficient power generation devices by applying a temperature differential across the device.

As with any new technology, product maturity will ultimately lower costs and drive market acceptance. Early adopters will utilize this technology based on its benefits and necessity. The obvious advantages are cooling density, reduced size and weight, extreme reliability, and precise temperature control. These advantages will lead to initial applications in remote land and space power generation, distributed power generation, and industrial power harvesting. Other uses will include military, industrial and consumer electronics cooling; and high-end electronics cooling such as servers, photonics cooling, and naval submarine cooling where noise reduction is crucial.

As volumes increase and the technology matures, thermotunneling device prices will drop and the market application space will broaden. Cooling applications will include commercial space cooling and refrigeration, residential refrigerators, freezers, air conditioners, and dehumidifiers. Automotive interior cooling and transport refrigeration are additional potential markets. Power generation opportunities exist in remote stationary power driven by geothermal, solar, or fossil fuel sources. Another area is portable power for electronic devices utilizing a combustible, gas-driven thermotunneling energy cells. Thermotunneling devices for waste heat energy recovery will find uses in power generation, as well as automotive, trucking, industrial, and agricultural vehicles. Alternate uses will be in permanent implantable power generation for medical devices, taking advantage of the temperature differential between the body and the surrounding environment. The total market opportunity for thermotunneling-based systems is estimated in excess of $45 billion.

Budget Period:

 The budget period breakdown by government and cost share dollars per period is shown in table1.

Table 1 – Project Funding Profile

	BP#1		BP#2		BP#3		Total	
	Gov. Funding	Cost Share	Gov. Funding	Cost Share	Gov. Funding	Cost Share	Gov. Funding	Cost Share
GE Global Research	$516,907	$262,994	$475,933	$242,147	$507,160	$258,035	$1,500,000	$763,176
Total:	$516,907	$262,994	$475,933	$242,147	$507,160	$258,035	$1,500,000	$763,176
CS %:		33.72%		33.72%		33.72%		33.72%

Program Description

   The program description can be found in the Budget Periods Overview and Deliverables section). Work and accomplishments on each of the major tasks will be covered in the following sections.

Task 1: Investigate device architectures

Physics based modeling

 The purpose of modeling the tunneling "sandwich" is to give us guidance concerning materials and dimensions we may wish to use in experiments, answer other questions, and increase the likelihood of good results. However, we should understand that QM (quantum mechanical) calculations of macroscopic systems such as ours rarely give very quantitative answers because quantum phenomena are exquisitely sensitive to material details at the atomic level, and these are very difficult to know and control. Examples of things that we may not know well are:

- the exact arrangement of atoms at the surfaces and interfaces (e.g., interface roughness)
- the level and type of contamination/impurities in the materials and at the surfaces/interfaces
- charge accumulation at the interfaces
- penetration of the electric fields into the metals
- band structure effects (e.g., knowing correct effective masses)
- inelastic tunneling

- Changes in the parallel (to the interface) components of the electron momentum or wave vector (usually called $k_{||}$). It is usually assumed that this is continuous across the interface, but inhomogeneities may make this not so.

Therefore, the equations are more likely to give us useful qualitative guidance. It may be that we can calibrate some equations with experimental data to make the results more quantitative.

The tunneling model that most closely matches our situation is the metal-insulator-metal junction. Highly doped Si can approximate a metal if we use that on one side, we may evaporate a metal onto the other side, and the insulator in between can be either a vacuum or the insulators which we have discussed using (SiO2, Al2O3). The tunneling formula for this case is:

$$j = (2e/(2\pi)^2 h)\int dE \left[f_L(E) - f_R(E+eV) \right] \int d^2 k_\Pi D(E, k_\Pi)$$

$$where:\hspace{6cm}(1)$$

$$f = \left[1 + \exp((E - E_F)/k_B T) \right]^{-1} = Fermi\ function$$

$$E = E_x + E_\Pi$$

$$E_\Pi = \eta^2 k_\Pi^2 /(2m)$$

and where:

j = transmitted current density

D = j/j₀ = transmission probability through the tunneling barrier

j₀ = current density incident on the tunneling barrier

e = electron's charge = 1.6022E-19 coulombs

h = Plank's constant (bar denotes division by 2π) = 6.6256E-34 J-s

E = electron's energy (measured with respect to the bottom of the conduction band in the left metal)

k=electron's wave vector

x=direction perpendicular to the junction interfaces

y,z are the directions parallel to the junction

E_F = Fermi energy (Note that it is equal for the left and right metals if they are in tunneling contact.)

k_B = Boltzmann's constant = 1.3805E-23 J/K

Subscripts L,R denote left and right sides of the junction.

m= effective mass of the electron in the metal (free electron mass = 9.1094E-31 kg)

D is usually regarded as not being a function of $k_{||}$. Then Eq. (1) becomes:

$$j = \int_0^\infty dE_x D(E_x) N(E_x) \tag{2}$$

$where$

$$N(E_x) = (4\pi me / h^3) \int_0^\infty dE_\Pi (f_L(E) - f_R(E + eV))$$

$$D(E_x) = \exp[-2\int_{xL}^{xR} dx((2m_b)^{1/2} / \eta)(U(x) - E_x)^{1/2}]$$

Here U(x) is the potential energy of the tunneling barrier. xL and xR are the locations where the electron enters (on the left, xL) and leaves (on the right, xR) the tunneling barrier; i.e., where $E_x=U(x)$. m_b is the effective mass of the electron within the barrier, and this would be the free electron mass = m_e if the barrier is vacuum or some other value if it is an insulator, such as an oxide. Taking the zero of energy at the bottom of the conduction band of the left metal, U(x) is often given by (We will use SI [MKS] units throughout this work.):

$$U(x) = E_F + e\phi_{mL} + e(\phi_{mR} - \phi_{mL})x/w - eVx/w - e^2w/(16\pi\varepsilon x(w-x))$$

where (3)

$$\phi_{mL,R} = left, right\ metal\ work\ function\quad (in\ volts)$$

$$\varepsilon = permittivi\,ty\ of\ the\ barrier$$

$$w = barrier\ width$$

The last term above is the image potential of the electron in the metal and is often called the Schottky effect. If the barrier is an insulator, then ϕ should be replaced in the equations by ϕ-χ, where χ is the electron affinity of the insulator (the voltage difference between the conduction band and vacuum) at the L or R interface.

Equations 2 and 3 must generally be solved numerically, but they can be solved analytically in some limits. These give good qualitative guidance to the experimenter. For small V (such that the barrier is trapezoidal) and the electrons tunnel from the left metal into the right, the result is:

$$j = (4\pi me\ D_0/2h^3)V(2E_F - eV) \qquad (4)$$

$$where\quad D_0 = \exp(-(2m_b e\phi_A)^{1/2}2w/\eta),\quad small\ V$$

$$\phi_A = (\int_0^w dxU(x,V=0))/ew \cong (\phi_{mL} + \phi_{mR})/2$$

Here D_0 is an evaluation of D obtained using the WKB approximation. We see that for eV<< E_F, the current density J looks ohmic.

When V gets larger such that the barrier becomes triangular, the electrons are injected into the barrier, which is either a vacuum or insulator. In this case, the result becomes that for Fowler-Nordheim tunneling, also called field emission or cold-cathode emission:

$$D_0 = \exp(-4(2em_b)^{1/2} \phi_{mL}^{3/2} / 3\eta V), \quad l \arg e \quad V \qquad (5)$$

In this large V limit for j, we see an exponential dependence on V. Note that, in Eq. 5, $V=\Phi_{mL}/w$ when the electron tunnels into the collector electrode, which would give a formula for D_0 which differs from that of Eq. 4 by a numerical factor 4/3 instead of 2. This is probably due to approximations used in calculating the tunneling matrix element, and I have found empirically that reducing the 2w in the exponent of D_0 of Eq. 4 by a factor 1.25 will recover Φ from the integral calculation accurately.

      It seems likely that we will be wary of the large V regime, since we will be getting close to voltage breakdown (arcing). Also, as we shall see, this regime is probably less efficient.

Thermionic Emission:

      When the energy of an electron (E_x) is above the tunneling barrier U, it can cross the junction freely, without tunneling. This situation is called thermionic emission. It is described by the Richardson-Dushman equation, which can be derived directly from Eq. 2 if we set D=1 for this case ($E_x > U(x)$ everywhere). The result is:

$$j = (4\pi me(k_B T_L)^2 / h^3) \exp(-U_{max} / k_B T_L)$$
$$- (4\pi me(k_B T_R)^2 / h^3) \exp(-U_{max} / k_B T_R) \qquad (6)$$

where U_{max} is the maximum of U(x) over the barrier width, 0 to x, and where we have let V=0.
Therefore, our equations include this standard formula for thermionic emission. Notice that when $T_R>T_L$, the net emission goes from the hot side to the cold side,

as one would expect. Therefore, since we are trying to drive current from the cold to the hot electrode, thermionic emission hurts us and must be overcome by a non-zero V. It is unlikely to occur in any appreciable amount at these ambient temperatures unless the work functions are very low. In the literature, small changes are often put into the Richardson-Dushman equation to increase accuracy by adding quantum reflection by the barrier and modification of the barrier function by temperature and surface irregularities. Since we expect small contributions from this effect anyway, we do not bother with such corrections.

Cooling Power and Efficiency:

The power consumed by the junction is merely jV per unit area. How much energy is transported across per unit time (cooling power, in watts/m^2)? To calculate this, we should just substitute (E-E$_F$), the energy of each tunneling electron with respect to its average replacement electron energy, E$_F$, for its charge. Using Eq. 2, we get:

$$cooling \ power = C =$$

$$\int_0^\infty dE_x D(E_x)(4\pi m/h^3)\int_0^\infty dE_\Pi (E - E_F)(f_L(E) - f_R(E + eV))$$

$$coefficient \ of \ performance = COP = |C|/jV$$

$$COP \ vs \ Carnot = (|C|/jV)(T_L/T_R - 1) \qquad (7)$$

Here C will appear as a positive (negative) number if the left metal-emitter is being cooled (heated). This result can be adjusted for the establishment of a non-equilibrium temperature situation (L metal cooler than R) by substituting 2 different temperatures, T$_L$ and T$_R$, into the respective Fermi functions, f, before performing the integrations.

Commercial home refrigerators today can work between -13 and 105 F (248 and 314K), and they remove about 234 W. Their current COP is 1.62, and their Carnot efficiency is 43%.

Parameters we may wish to vary and starting values:

$E_F \sim 10$ eV (May vary it 4-15 eV, but it should not have much effect; 1eV=1.6021E-19 J)

$\phi_{mL,R} \sim 1$ volts (Will probably want to vary this in the .5-3 volt range.)

w ~ 4 nm (Vary this 2-10 nm.)

V ~ 1 volt (Vary 0-5 volts.)

m, m_b ~ Use free electron values to start. Can vary these down to $.1m_e$.

$\in$ ~ Use permittivity of free space for a vacuum = 8.8542E-12 farads/m. In the barrier, this can be varied to a value ~10X higher.

$T_{L,R}$: If the ambient temperature around a refrigerator is ~70F, the cooler must discharge heat at ~ 90F. The cold end is at 0F (make it –5F for efficiency). So T_R~305K and T_L~250K. Appliances tells us that the freezer cold-side temp is –5F and the hot side is 55-110F (285-316K).

Print out: electric field in the junction = V/w

Parasitic losses:

Parasitic losses are undesired thermal "leaks" which decrease the efficiency of the device.

When we use vacuum alone as the tunneling gap, radiation loss (as thermal backflow across the gap) is still present. For emitter and collector temperatures of 250K and 305K and an emissivity of .5 (which may be considerably lowered for shiny metals), this loss is ~130 W/m^2, which can be overcome by reasonable cooling powers.

Using solid insulating materials as the barrier has severe consequences for parasitic thermal losses. For example, using SiO_2, which has a thermal conductivity K = 1.3 W/mK (fully dense), allows a leak of 1.2E10 W/m^2 for a barrier thickness of 6 nm. This is probably unacceptably high for any reasonably achievable cooling power. Even using a gas within the gap is not good. For example, the best inert gas is xenon, with a conductivity of .0056 W/mK, which still gives a leak of 5.1E7 W/m^2 under the conditions stated above. One can ameliorate the thermal effect of a solid barrier by reducing the area (footprint, or width) of the barrier between the two electrodes, leaving the remaining area as vacuum. If a cooling power C can be achieved by tunneling in a given device, one desires to keep the thermal "backflow" to a fraction f of C. The thermal "backflow" conduction (watts per unit area) across the barrier "posts" is K(Tr-Tl)(Ap/Ad)/w, where Ap is the area of the posts and Ad is the area of the device. We then get this formula for determining the fractional post area allowed to keep the backflow at the restricted value:

$$A_p / A_d = pCw / (K(T_R - T_L)) \qquad (8)$$

As an example, if p=1%, w=6 nm, C=26E4W/m2, K=1.3 W/mK (for SiO2), and (Tr-Tl)=55K, we get Ap/Ad=2.2E-7. For a 1 mm2 device, this means that Ap=2.2E-13 m2 at most. That allows one post with radius ~260nm (or multiple posts adding up to the same area.

Another unavoidable parasitic is ohmic loss in the emitter side of the junction. Since some current density j is flowing through the junction during operation and since the cold (emitter) side metal will have some electrical resistivity ρ, there will be some ohmic heating of the cold side (=$j^2 \rho t$ W/m^2, where t is the thickness of the emitter metal). For good metals like aluminum (ρ=2.65E-8 ohm-m), this will be a small number; e.g., for J=1E6 W/m^2 and t=1E-4 m, the heating is ~2.6 W/m^2.

Finally, the connections of the cold section (emitter) to the outside will constitute parasitic leaks of some size. Examples are the electrical connection to the power source and structural/frame supports. These can be minimized.

Other physics issues:

There are statements in the literature (e.g., Chung et al., J Vac. Sci. Tech. 12, 727 (1994); Cutler et al., Appl. Surf. Sci. 76/77, 1 (1994)) that the replacement electrons from the wire connected to the emitter do not arrive with an average energy at the Fermi energy but lower. If this is the case, the operation of the tunneling sandwich is more favorable. Chung et al. claim the replacement energy is 10-100 meV less than E_F. I have run a case for replacement at 50 meV less, and it gives an increase in the cooling power, and the COP vs Carnot increases ~15%. Since I do not agree completely with the physics Chung et al. are using and since others in the literature do not claim this credit, I will be conservative and not claim it.

Power generation:

As with all such devices, the TT sandwich will generate power when a temperature gradient is maintained by some means across the sandwich. The same equations given above can be used to calculate this case. When Eq. 2-3 are solved for V=0, one obtains the maximum current flow which the device will provide, which is against a zero voltage load (closed circuit). When V is increased until j=0, that V is the maximum voltage which the device will produce (in open circuit). The maximum power the device will produce is the maximum of jV, which occurs between these 2 values. The efficiency of the device is jV/C, since, in this context, C is now the net heat energy carried by the electrons from one side of the junction to the other. The Carnot efficiency of a heat engine

working from the hot side (T_R) to the cold side (T_L) is $1-T_L/T_R$. Therefore, the efficiency vs a Carnot heat engine is $jV/(C(1-T_L/T_R))$.

Of course, a TT device used for heat generation is subject to all the same parasitic loses as a refrigeration device. For example, maintenance of the thermal gradient (T_R-T_L) requires that the conduction of the thin TT junction be minimal.

Thermoelectric (TE) effects:

In principle, we should also consider standard TE effects <u>if</u> our electrode materials are different. In that case, they will have different Peltier coefficients, P_L and P_R, where L and R represent the left and right electrodes. By the usual operation of thermoelectrics, the junction will absorb a heat-per-unit-area of $J(P_L-P_R)$, where J is the current density flowing from right to left. As usual, the same heat will be discharged at the other junction between the 2 materials. The picture may be complicated by having more than two materials in the circuit; e.g., wires of a third material are attached to the 2 electrodes. However, the same formula applies for the heat absorbed or created at each junction. (For reference, $P=ST$, where S = Seebeck coefficient.)

Since TE effects are generally quite small between most materials, the Peltier effect will be a small correction if the TT effect is working well at a given junction. However, the point is that simply by passing the current in the proper direction, we can add this effect to TT rather than having it subtract from it.
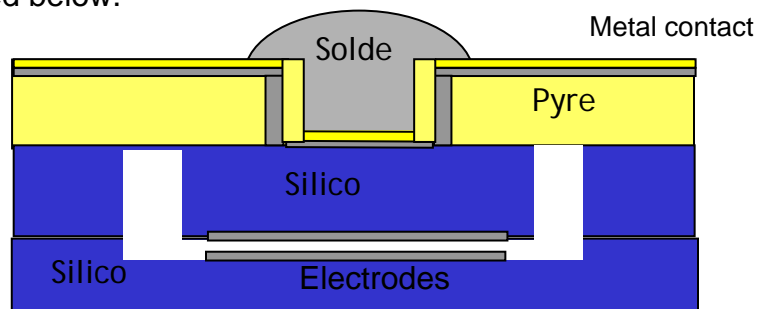
Device Design

The team conceived a total of nine architectural concepts. Using GE's proprietary six sigma tools the nine concepts were traded off against a set of "Critical to Quality" parameters. These parameters included total system

efficiency, cooling power density, maximum device size, reliability, manufacturability, environmental impact, work function requirement, cost and intellectual property potential. The tradeoff was based on our qualitative and in some cases quantitative understanding of the device structures and physics. From this study 3 potential device architectures were chosen and carried forward for thermal and structural analysis.

Thermal modeling of the proposed structure is essential as it relates directly to the efficiency of the end device. Device design and material composition contribute to the thermal back path of the device and are therefore important factors. In addition to thermal modeling, structural modeling is used to predict the maximum device size and device reliability. The thermal study focused on emissions through a vacuum gap. This is required to avoid conduction heat transfer in the gap, which leads to decreased device efficiency. Additionally the conduction contribution due to the external support structure was modeled. Structural modeling included the effects of external atmospheric pressure that causes bending of the devices. Besides deflections due to pressure gradients, numerical models through Finite Element Models were extended for thermo-structural effects due to the CTE mismatch of the materials and processing temperatures.

Several jugular experiments were also carried out to investigate the feasibility of fabricating the proposed structures. Based on these experiments and the thermal and structural modeling a single device design was chosen. The design concept is depicted below.


Down selected device design

. This design approach utilized commercially available highly doped silicon wafers and pyrex. The construction was accomplished using a combination of standard and modified, silicon wafer, and MEMs, fabrication techniques.
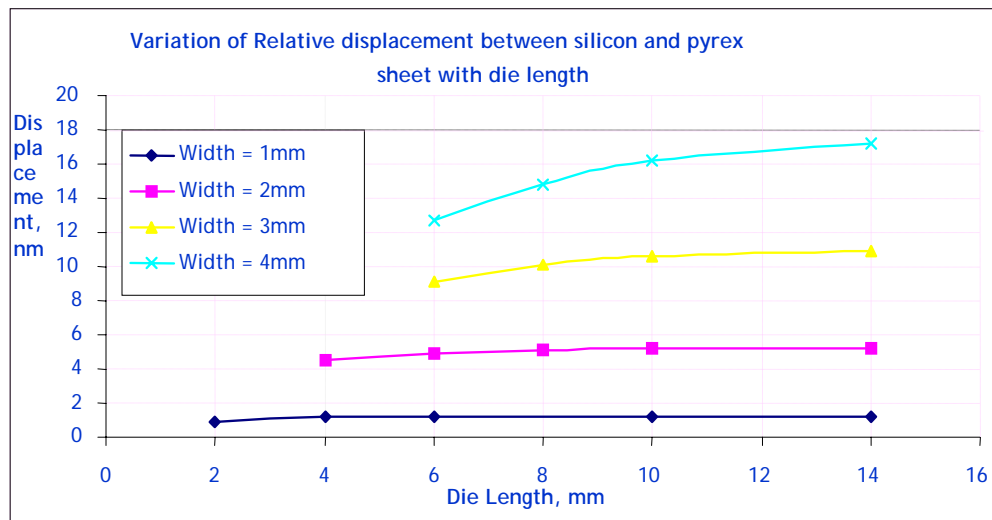
Extensive thermal and structural modeling efforts going forward concentrated on the down selected design. A two dimensional axi-symmetric "ANSYS9.0" thermal model was created to understand the thermal performance. The results show that more than ~85% of the tunneled heat can be rejected to the ambient while ~15% or less returns to the cold electrode through conduction paths at the exterior of the device.
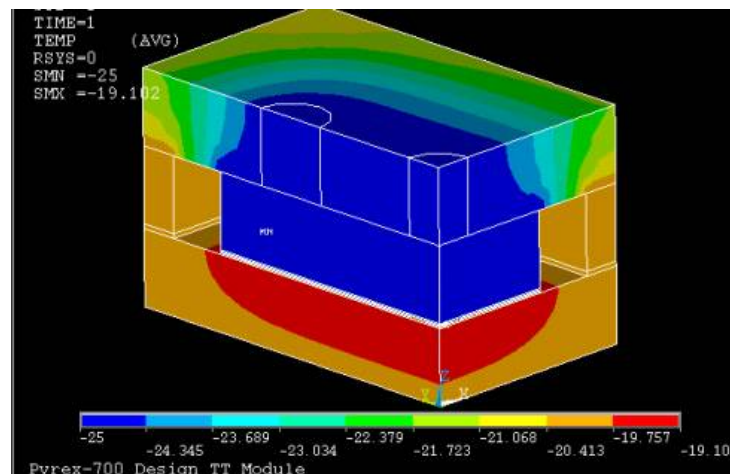
Since the design was expected to provide good thermal performance, further analysis was performed to better understand the other parameters affecting the design. Effect of the external heat transfer on the parasitic back heat flow is given below. It is shown that heat should be removed with a forced convection heat sink to decrease the parasitic losses. Having better heat transfer modes such as dielectric liquids or water-cooling can provide better performance.
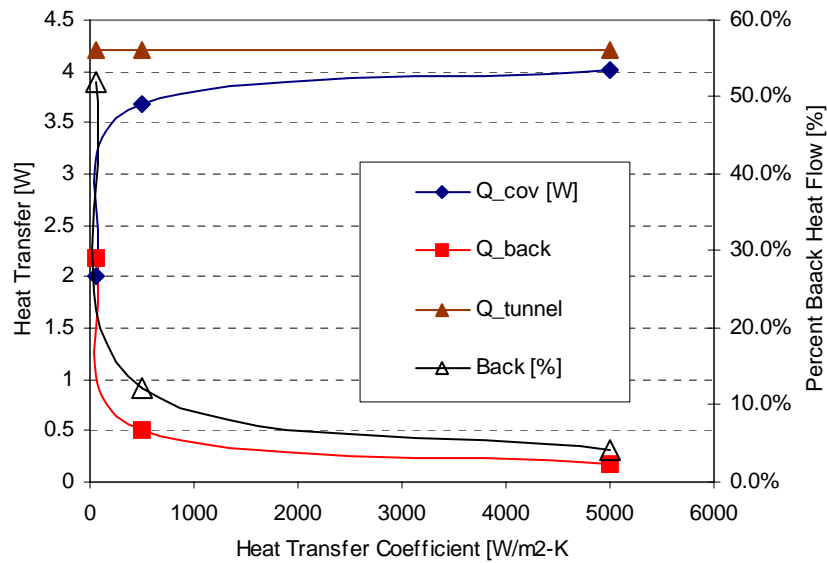
In addition to thermal modeling, structural models were created to understand the local deflection effects in the device due to CTE mismatch, fabrication, and atmospheric pressure. To avoid or decrease the deflections smaller devices are necessary and the preferred shape is a rectangular or long narrow device.

The figure above represents the structural modeling for some typical rectangular module structures as a result of the atmospheric deflection.

In addition to the thermal and structural concerns, parasitic losses due to electrical resistances along the electrical path were minimized by optimization of the metal thicknesses, wafer doping and current spreading along the tunneling electrodes. Optimization trade offs between the metal thickness and roughness were conducted.

Another issue uncovered early in 2006 was the debate over the transmitted radiation across nano-sized vacuum gaps. A literature search was completed and a total of nine journal papers were identified, 8 theoretical, one experimental. The reported values ranged by 5 orders of magnitude, with a mean value for a device of our type being ~.1W/cm-K or a system efficiency loss of ~17%. Several experiments were conducted to determine the actual nano-radiation contribution. Samples of the proposed structure were fabricated and measured for mass, specific heat and thermal conductivity. Two separate methods were used to determine the thermal conductivity of the devices, Laser diffusivitivity and steady state thermal transfer. Additionally the same measurements were made on each of the individual components that make up the device and an ANSYS finite element thermal model was constructed using the measured values. The difference between the model and the actual device thermal conductivity would be the nano-radiation component. Laser diffusivity was the first method examined. After careful study of the results it was determined that the laser diffusivity approach was faulted as the response time of the IR detector was unable to resolve the photon contribution of the nanoradiation and thus unreliable results were obtained. Efforts were then concentrated on the steady state measurement techniques. In this experimental setup shown below the device is sandwiched in the structure and a steady state delta in temperature is created using the heater and thermoelectric cooler. The fixture is placed in a vacuum vessel and surrounded with an IR reflector. Careful measurements of the temperatures and applied flux are made and the

nanoradiation calculated based on the difference between the actual and modeled results. The measured results to date indicate values of 10-15W/mK. At these values efficiency reductions on the order of 30-40% are probable. Given this, efficient refrigeration via thermotunneling is not practical. Experiments however are continuing due to suspected errors that may be caused by the experimental setup compressing the gap.
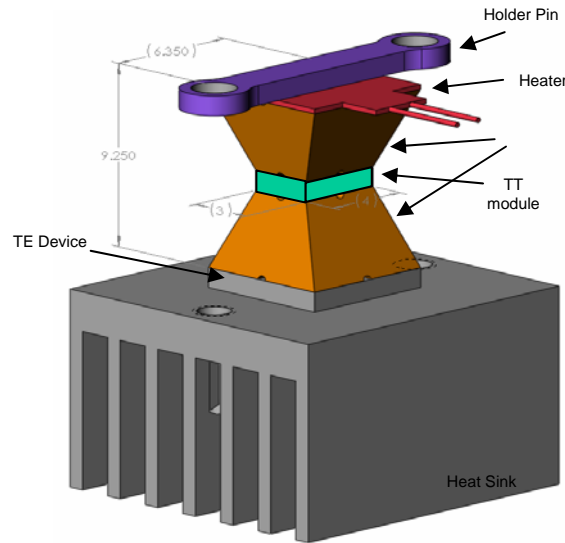

Device Fabrication

A lot of effort was spent investigating the fabrication of the proposed structure. The efforts were subdivided into the following device components to speed research. The components are as follows, pyrex via formation, pyrex solder via filling, electrodes, wafer bonding, and bottom silicon section.

Four techniques were investigated to explore forming the via thru-holes in the pyrex substrate. These methods were wet etching, mechanical drilling, microblasting and ultrasonic milling. Wet etching was eliminated due the long etch times and the inability of the etch hard mask to hold up during the etch. Mechanical drilling was eliminated due to the long serial drill times and the hole edge quality. Microblasting or micro sand blasting which involves abrading away the material using a fine particulate media and a hardmask on the substrate was investigated internally at GRC and externally with a US subcontractor. The internal effort involved constructing an automated blasting system and

developing an adequate hardmask technology. The automated system and an example via is shown below. Satisfactory vias have been demonstrated with the process and samples were used in fabrication. The external US subcontractor was eliminated due to the poor edge quality of the via due to undermining of the hardmask and break out at the via completion. Ultrasonic milling was also investigated utilizing a US based subcontractor. The pyrex is ultrasonically milled using a hardtool in a milling slurry. This approach was found to be satisfactory for forming vias and samples were used in device fabrication.
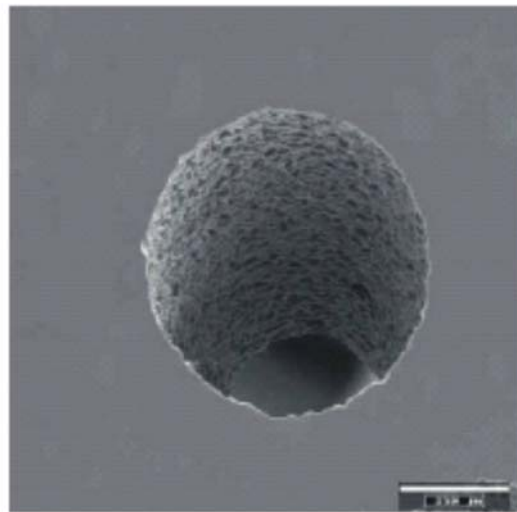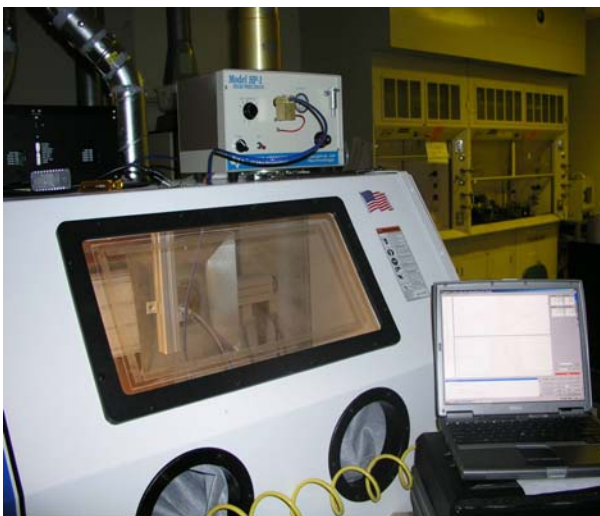
Automated micro blasting system, left and 500u micro-blasted via through pyrex

Once formed, the pryrex via wafer is then bonded to to the upper silicon electrode wafer using anodic bonding. The upper section then has the electrode material deposited, resist patterned and the resist in left in place for the deep etching of the silicon to form the isolation trenches.

The next step is fabrication of the silicon lower half of the device. Doping levels and types, for the silicon wafers, were chosen to address loss parasitics and possible dopant diffusion issues. Several metals and metal stacks were investigated for the electrodes. Ohmic contact and metal diffusion issues had to be addressed due to subsequent high temperature processing steps. A metal stack was identified to address all these issues. The gap is formed by first

forming a pocket in the lower silicon and then depositing and patterning the electrode metal stack. The difference in height between the pocket and the metal electrode stack forms the gap. In order to hermetically seal the top and bottom device halves, under vacuum, a proper material and process needed to be identified. Several sealing processes were examined and tested for device compatibility. The key issues were hermeticity, adhesion, processing temperature, induced stress, thickness control and uniformity. The process decided upon was a silicon-to-silicon low temperature diffusion bond. Several unique process steps were developed to allow consistent bonds at temperatures as low as 250C. Once bonded a solderable gold terminated metallization stack was applied to each of the wafer backsides, the vias solder filled, and the devices diced out.

One of hundreds, of prototype devices manufactured is shown below.
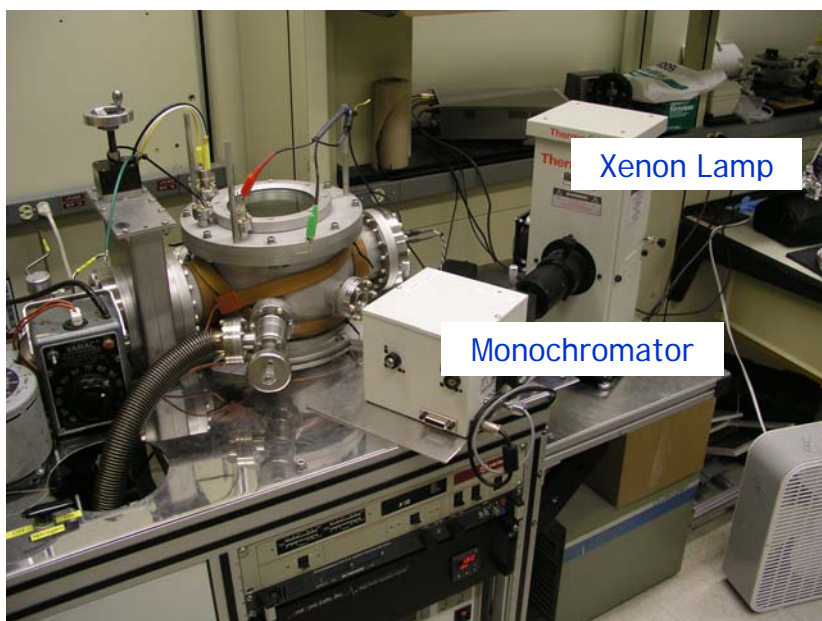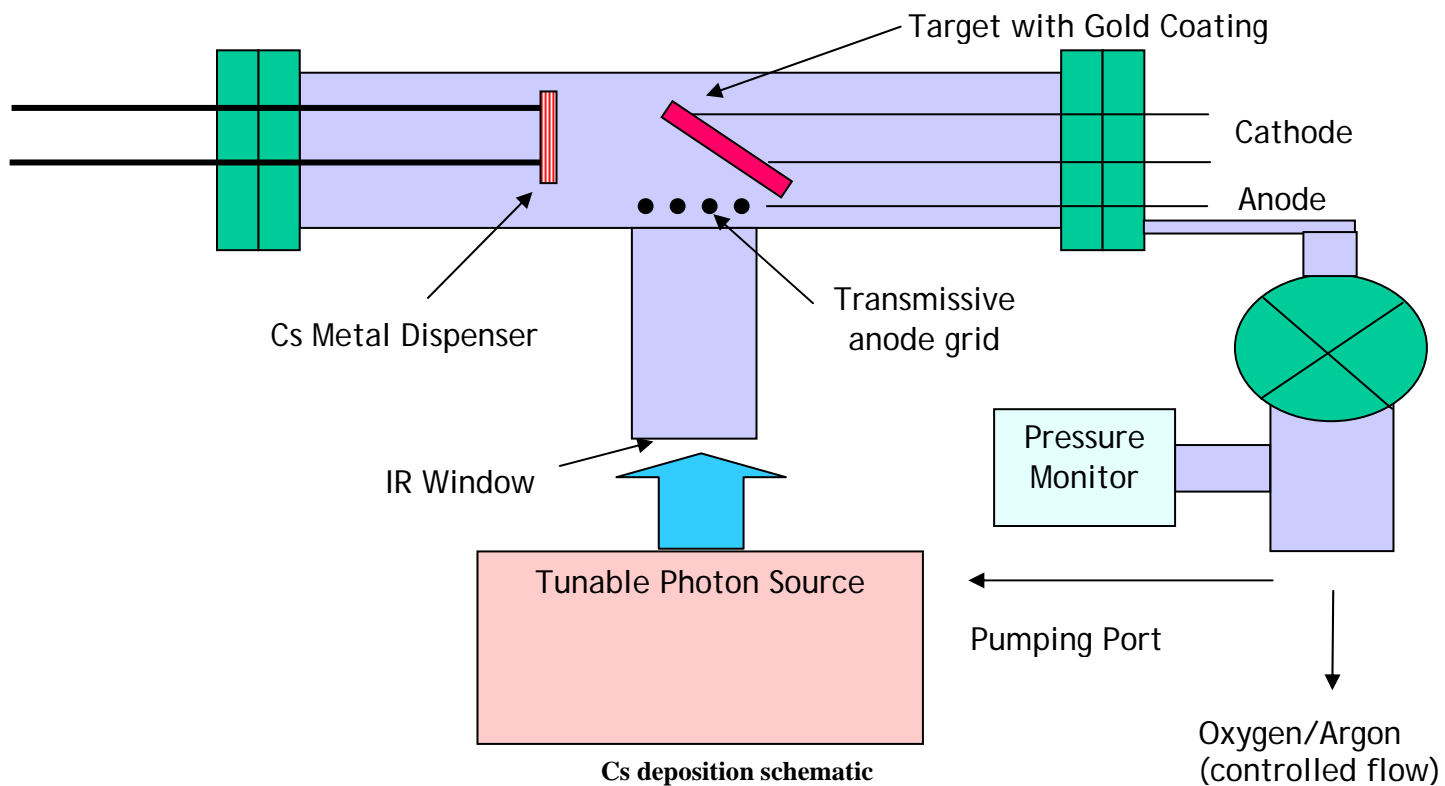

Low Work Function Materials

Low work-function materials are critical to the development of an efficient, viable thermotunneling device. In order to optimize critical operating parameters such as tunneling current density, cooling power and thermodynamic efficiency, electrode materials must exhibit very low energy barrier(s) to electron emission while remaining structurally and chemically stable. During the first and into the second year of the program several ultra-thin semiconductor candidate materials were identified for work function lowering. Deposition processes were developed for the candidate materials and characterization of these films regarding physical attributes such as adhesion and film roughness were completed. Additionally test
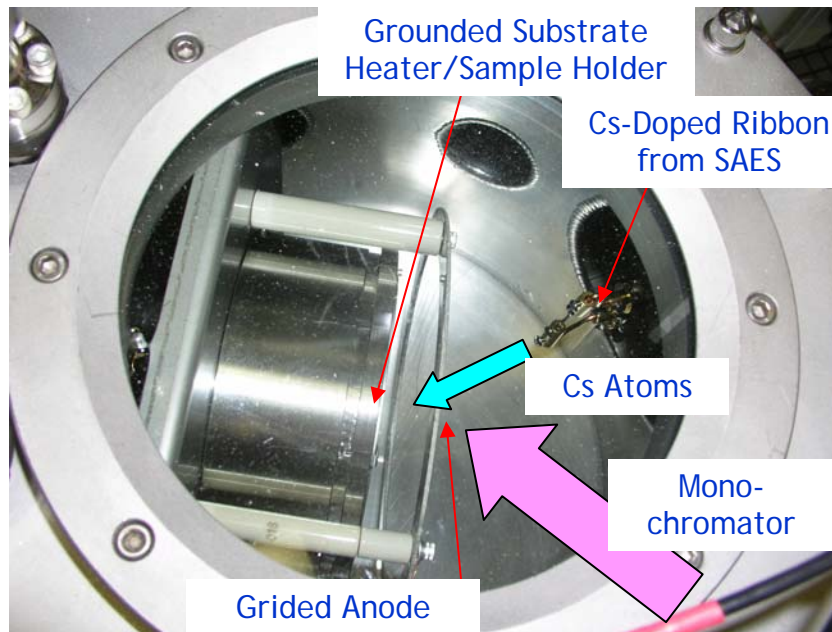
structures enabling characterization of the candidate materials at tunneling gaps of <10nm were designed and constructed. These test structures allow quick turn, low cost testing of potential materials in a device that is very similar to the chosen architecture. The data from the IV curves of these test devices can then be fed into the device physics model to generate an effective work function. This work continued into 2006 resulting in the identification of 2 potential materials that were measured to have "effective" work functions of 0.75eV and 0.85eV. The key caution with these materials is that the physics model used to calculate "effective" work function utilizes a beta term equal to 1, and thus rougher surfaces would result in a lower effective work function and reduced tunneling area. Although low work function values were obtained, these materials are unconventional and much is unknown about their performance until they are tested in actual prototypes. Therefore the team also decided to investigate more conventional proven material systems during 2006 to 2007.

The bulk of the conventional low work function effort was concentrated on oxygenated cesium metallic alloys. These alloys were identified in literature dating back to the 1960's and were mainly used in IR detector vacuum tubes. Values as low as 0.65eV were cited for oxygenated gold cesium alloys. This coating was targeted first for investigation due to its extremely low work function and its reported stability. Given this, a used vacuum system was purchased and modified to allow the deposition of cesium on heated, gold coated substrates at vacuum levels in the 10-7 to 10-9 Torr. Additionally a broadband scanning monochromator and current collection system was designed and built to allow monitoring of the work function at incremental steps during the cesium deposition. The capability to oxygenate the Au/Cs alloy was also added to the system. A commercially available metal infiltrated cesium source was identified and obtained from SAES getters. The source is relatively stable at atmospheric conditions and releases cesium under vacuum by current heating. A schematic of the design of the deposition system can be seen below, and the actual system in the following figure.

Work Function Measurement

Target with Gold Coating

Cathode

Anode

Cs Metal Dispenser

Transmissive anode grid

IR Window

Pressure Monitor

Tunable Photon Source

Cs deposition schematic

Pumping Port

Oxygen/Argon (controlled flow)


Xenon Lamp

Monochromator

**Cs deposition system and close up of deposition chamber**

To complete the system, automated data acquisition was added, to enable control of the scanning monochromator and to collect current data from the grided anode. Baseline calibrations were performed to quantify pumping speed, cesium emission rates, work function measurement of known materials and the overall system sensitivity. Experiments were run looking at the various process parameters such as Cs deposition time, and temperature vs. photoemission yield.

As seen in the IR photoemission signal graph in the figure below, work function values of less that one electron volt have been achieved. The work function of bare gold is ~4.8eV. The next step is to finish completion of the modified wafer bonder to allow insitu Cs deposition and wafer bonding so as not to expose the Cs to atmospheric conditions. This work is continuing through the end of 2007.
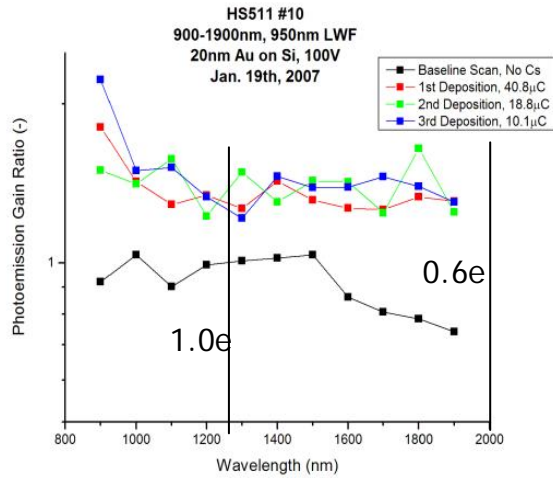
Cesiated Gold work function measurement

A second Cs deposition system was also constructed to investigate the effects of Cs on emission under high electrical fields. This was necessary, as the actual device prototypes will function in this mode as opposed to photoemission. The system diagram is shown below and allows Cs deposition, photoemission and high field-testing all without breaking vacuum.
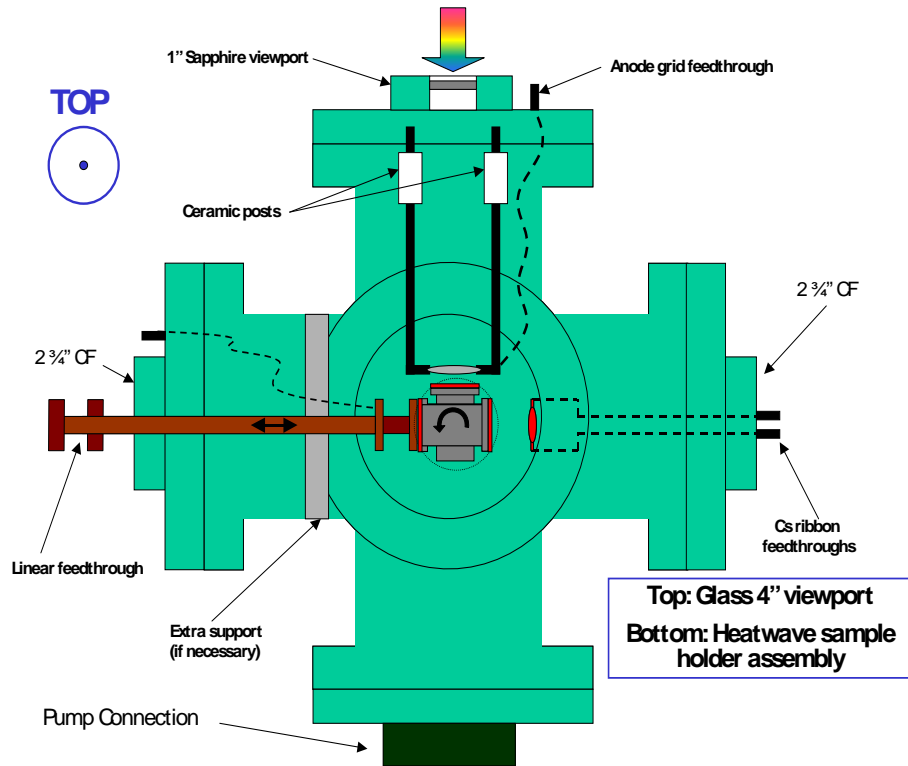
High field-testing was conducted and enhancement in emission was shown after Cs deposition. Unfortunately accurate calculations of work function could not be made, as the actual emission area was unknown. Test data is shown below, the baseline condition is prior to Cs deposition.
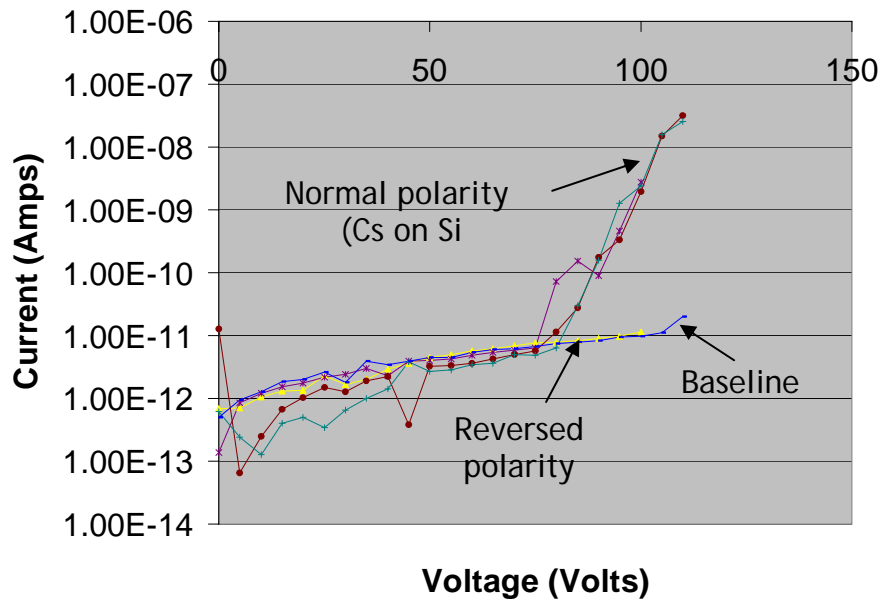
A series of tests are performed to downselect the best prototypes. The first test is an ultrasonic scan of the devices in wafer form that looks for the presence of the gap and sealing of the bond edges. No numerical value of the gap is obtained. The second test is a voltage current measurement that looks at the values of currents as the device is run through a series of voltages. The best devices are chosen based on the highest current values in the linear portion of the tunneling curve. Next these devices are run through a laser vibrometry test which subjects the device to a high frequency AC signal bringing it into mechanical resonance while the device is observed with a laser vibrometer. From this test a rough value for the gap size is obtained as well as verifying the symmetry of the gap movement. Stuck electrodes can be seen from this test. A good and bad device is shown below.
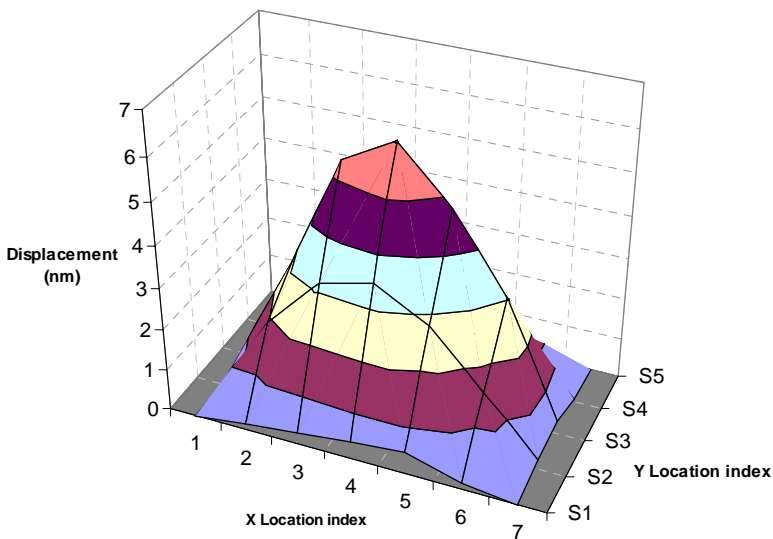

Good device
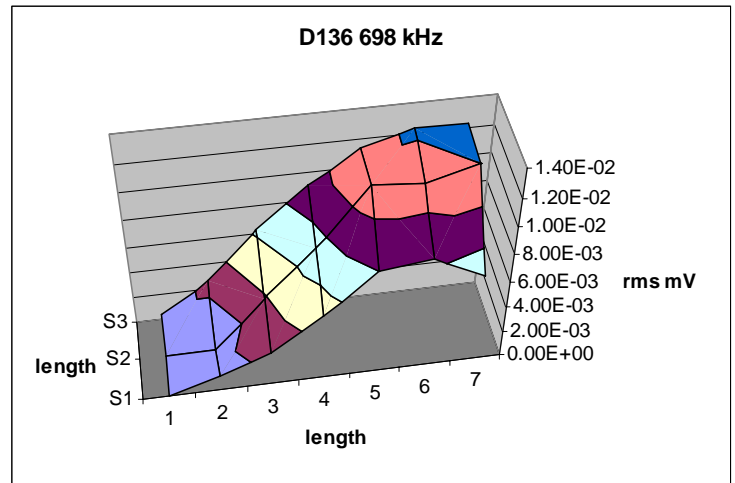
Electrode bonded on

Following the laser vibrometry test the prototypes are then passed on for a power generation testing by applying a temperature differential across the device at an optimum resistive load. The power generation test further verifies device functionality with the caveat that not all good power generation devices will make good cooling devices. This can occur when the gap size is less than 4nm. Finally the downselected devices are sent for cooling testing. A custom device test rig was constructed to test devices in vacuum while allowing monitoring through electrical connections, thermocouples and viewing with an IR camera. A photo of the actual test setup is shown below. The device holder shown on the right allows viewing of either one side of the device or simultaneous viewing of both sides with the IR camera.
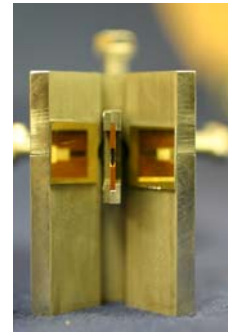

Photos of custom vacuum test setup with IR camera

As of this date only "dynamic" low work function electrodes have been tested. Several of these prototypes were tested in the one sided and two side configuration. In the two sided configuration no heatsinking is provided so cooling is not anticipated. This test is conducted to look for differential heating of the electrodes, which is an indication of tunneling and possible cooling. Following this test the devices are mounted for single sided cooling testing. In this configuration one side of the device is mounted to a heatsinked thermoelectric cooler and brought to a stabilized temperature. The device is then run through a series of voltages while the temperature of the non heatsinked side is tracked with the IR camera. The viewed side temperature dipping with the application of power would indicate cooling. To date no cooling has been observed in any of the prototypes tested. Differential heating of the collector electrode has been observed and calculations of the differential heating show definitive proof of tunneling within the device. Testing of devices will continue through 2007 with Cs samples being done before the years end. Several speculations as to why cooling has been not observed have been made to date. Firstly the experimental nanoradiation values measured are excessively high and would reduce the total cooling powers and efficiencies to very low undetectable levels. Additionally the prototypes tested to date have used the controversial dynamic low work function materials and although the current density was shown to increase with the use of these materials, the electron energies emitted from them are unknown. Lastly the actual tunneling area in the prototypes is unknown and so the cooling power density is for a given are is unknown as well at the electron energies for the area. A sample double and single sided image from the IR test setup is shown below.
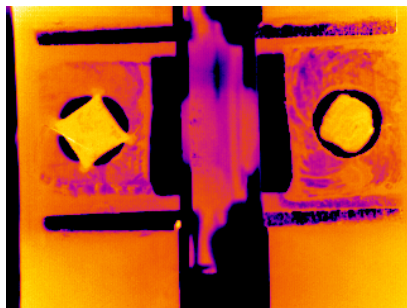
2 sided IR
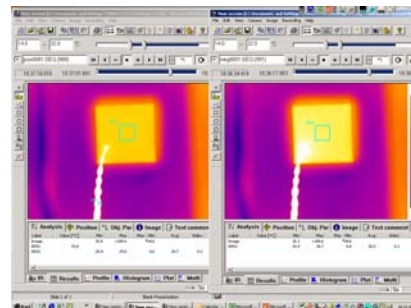
1 sided IR

Budget Periods Overview and Deliverables: The inter-relational dependency schedule is shown in the project Ghant chart below.

PROPOSED WORK PLAN, SCHEDULE, AND MILESTONES

Program Activities	Year 1 Q1	Q2	Q3	Q4	Year 2 Q1	Q2	Q3	Q4	Year 3 Q1	Q2	Q3	Q4
Task 1 Investigate device architectures.												
1.1 Device modeling.												
1.2 Screen architectures.												
1.3 Conduct jugular experiments.												
Milestone: Defined architecture.												
Task 2 Develop low work function electrodes.												
2.1 Modify device model.												
2.2 Screen materials.												
2.3 Device-level jugular experiments.												
Milestone: <1.0 eV work-function material.												
Task 3 Design and fabricate device, modules, and subsystems.												
3.1 Device prototyping.												
3.2 Module/system modeling.												
3.3 Module prototyping.												
3.4 Subsystem prototype.												
Milestone: Prototype subsystem.												
Task 4 Demonstrate and optimize device, module, and subsystem.												
4.1 Test and optimize devices.												
4.2 Test and optimize modules.												
4.3 Test and optimize subsystem.												
Milestone: Optimized subsystem.												
Task 5 Program management.												